# Prediction of Steady and Unsteady Asymmetric Vortical Flows Around Circular Cones

Osama A. Kandil* and Tin-Chee Wong†
*Old Dominion University, Norfolk, Virginia 23529*
and
C. H. Liu‡
*NASA Langley Research Center, Hampton, Virginia 23665*

**Steady and unsteady, supersonic asymmetric vortical flows and their passive control around circular cones are considered in this paper. These problems are formulated by using the unsteady, compressible, single and double, thin-layer, Navier-Stokes equations. The equations are solved by using an implicit, upwind, flux-difference splitting, finite-volume scheme, either in a pseudotime stepping or in an accurate time stepping. An implicit, approximately factored, central-difference, finite-volume scheme has also been used to validate some applications of the upwind scheme. Local conical flows are assumed for the computational applications presented in this paper. Steady asymmetric vortical flows have been predicted by using random and controlled disturbances. Unsteady asymmetric vortex-shedding flows have also been predicted, for the first time, using time-accurate solutions with two different computational schemes. Control of flow asymmetry has been demonstrated computationally by inserting a vertical fin in the leeward plane of geometric symmetry.**

## Introduction

IN the high angle of attack (AOA) range, the separated vortical flow from forebodies of missiles and fighter aircraft may become asymmetric, producing large abrupt changes in force and moment coefficients. These abrupt changes may exceed the available controllability and lead to missile and aircraft spin. Experimental studies of several researchers[1-11] have identified four distinct flow patterns about slender bodies through a wide AOA range and zero-degree side slip. The first pattern develops in the very small AOA range, where the flow is attached and the axial flow is dominant. In the intermediate AOA range, the crossflow becomes of the same order of magnitude as that of the axial flow, the flow separates on the leeward side, and a symmetric vortex pair is formed. As the AOA reaches a high range, the symmetric vortex pair becomes asymmetric, and the flows stay steady. For this asymmetric vortex-flow pattern to occur, it is not a necessary condition to have asymmetric separation lines on the leeward side of the body. The fourth flow pattern develops at a very high AOA range, where asymmetric time-dependent vortex shedding occurs either randomly or periodically, similar to the von Kármán vortex street in two-dimensional flows around cylinders.

For isolated pointed forebodies, the onset of vortical flow asymmetry occurs when the relative incidence (ratio of AOA to nose semi-apex angle) exceeds a certain value; e.g., for a pointed circular cone, the relative incidence must be higher than two. However, the relative incidence value is not the only determinable parameter for the onset of vortical flow asymmetry. The onset of vortical flow asymmetry is also a function of the freestream Mach number and Reynolds number and the shape of the body cross-sectional area as well. Asymmetric vortical flow and vortex shedding have also been documented for delta wings[12,13] at very high relative incidences and low subsonic regimes.

For the critical values of the relative incidence, Mach number and Reynolds number, and the shape of cross-sectional area, the symmetric flow is unstable. Any small flow disturbance in the form of a transient side slip, acoustic disturbance, or similar source of disturbance causes flow instability that produces, depending on the flow conditions, either a steady asymmetric vortical flow or an unsteady asymmetric flow with vortex shedding. In this paper, we present an extensive computational study of the steady asymmetric vortical flow and unsteady asymmetric flow with vortex shedding to address some of the influential parameters as the relative incidence and Mach number.

As the experimental work shows, the mechanisms that lead to asymmetric vortex wake are not well understood. However, two mechanisms have been established for explaining the evolution of flow asymmetry.[5,6,9,10] The first mechanism applies to both laminar and fully turbulent flows. It suggests that flow asymmetry occurs due to instability of the velocity profiles in the vicinity of the enclosing saddle point that exists in the crossflow planes above the body primary vortices.[2,7,10] The second mechanism suggests that flow asymmetry occurs due to asymmetric transition of the boundary-layer flow either at the nose in the axial direction or on both sides of the body in the crossflow planes. For pointed slender bodies, the first mechanism produces higher side forces than those produced by the second mechanism. These results have conclusively been shown through the experimental work of Lamont[8,9] on 2-diam and 3.5-diam tangent ogive noses with cylindrical afterbody. An extensive review of the steady and unsteady vortex-induced asymmetric loads is given by Ericsson and Reding in Ref. 11.

Several attempts have been carried out to computationally simulate asymmetric vortical flows around slender bodies of revolution. Early computational work on conical flows has been published in Refs. 14 and 15. Graham and Hankey[16] presented the first three-dimensional Navier-Stokes computations for asymmetric flow around a cone-cylinder body at 30-

Received Jan. 2, 1990; presented as Paper 90-0598 at the AIAA 28th Aerospace Sciences Meeting, Reno, NV, Jan. 8-11, 1990; revision received Sept. 13, 1990; accepted for publication Sept. 17, 1990.


*Professor and Eminent Scholar, Department of Mechanical Engineering and Mechanics. Associate Fellow AIAA.
†Research Assistant, Department of Mechanical Engineering and Mechanics. Member AIAA.
‡Senior Research Scientist, Theoretical Flow Physics Branch. Senior Member AIAA.

deg angle of attack, 1.6 freestream Mach number, and $0.4 \times 10^6$ Reynolds number. The MacCormack explicit finite difference scheme was used for the computations on a relatively coarse grid of $26 \times 30 \times 60$. A very small perturbation is induced by the truncation error of finite difference algorithm that triggers an instability of the saddle point above the body (first mechanism for asymmetry). Hence, the instability is induced by numerical bias that is physically amplified to produce flow asymmetry. By switching the order of spatial differencing in the predictor and corrector sweeps, the asymmetry was reversed.

Degani and Schiff[17] used the thin-layer, Reynolds-averaged, Navier-Stokes equations to compute asymmetric vortical flow around an ogive-cylinder body. They found that flow asymmetry can be obtained by introducing an asymmetric disturbance very close to the body nose. The disturbance they used was in the form of a small jet that was blown from one side of the body near the nose. However, when the jet was turned off, the numerical solution unfortunately showed that the flow recovered its symmetry. The authors of the present paper believe that the problem is attributed to the smallest scale of the grid at the solid boundary and the damping effect of the numerical dissipation in the axial direction, in addition to the grid-fineness distribution.

Marconi[18] used the Euler equations to solve for supersonic flow past a circular cone in conjunction with a "forced separation model," which was used by Dyer, et al.[19] The pseudotime stepping was carried out until the residual error reached machine zero while the flow was symmetric. Proceeding with the time stepping, vortex-flow asymmetry was obtained and stayed stable thereafter. It is believed that the asymmetry was triggered by the machine round-off error, which acted as a disturbance to the saddle point in the flowfield. In a later paper, Siclari and Marconi[20] used the full Navier-Stokes equations to solve for supersonic asymmetric flows around a 5-deg semiapex angle cone over a wide range of angles of attack.

Very recently, Stahl[21] conducted experimental studies of the low-speed flow around a circular cone of 8-deg semiapex angle circular cone in the angle of attack range of 15–50 deg at a Reynolds number of 7800 based on the base diameter. The onset of flow asymmetry was observed at 35-deg angle of attack. He has shown that the flow asymmetry can be suppressed by inserting a fin along the leeward plane of geometric symmetry with its edge along a ray through the apex. The minimum fin height for this purpose was found to be equal to the local radius of the cone.

In this paper, the supersonic, steady and unsteady, asymmetric vortical flows around circular cones are studied using the unsteady, compressible, single thin-layer, Navier-Stokes equations. Two computational schemes are used to solve the equations. The first, which is the main scheme used in this paper, is an implicit, upwind, flux-difference splitting, finite-volume scheme. The second, which is used to validate certain cases of the upwind scheme, is an implicit, approximately factored, central-difference, finite-volume scheme. Pseudotime stepping is used for steady flows and time-accurate stepping is used for unsteady flows. Some of the influential parameters for flow asymmetry, such as the relative incidence and Mach number, are addressed. A flow case of passive control of flow asymmetry is also studied using the unsteady, compressible, double thin-layer, Navier-Stokes equations.

## Formulation

The three-dimensional compressible viscous flow around the body is governed by the conservative form of the dimensionless, unsteady, compressible, double thin-layer, Navier-Stokes equations. In terms of time-independent, body-conformed coordinates $\xi^1$, $\xi^2$, and $\xi^3$, the equations are given by

$$\frac{\partial \bar{Q}}{\partial t} + \frac{\partial \bar{E}_s}{\partial \xi^s} - \frac{\partial (\bar{E}_v)_2}{\partial \xi^2} - \frac{\partial (\bar{E}_v)_3}{\partial \xi^3} = 0, \qquad s = 1,2,3, \tag{1}$$

where

$$\bar{Q} = \frac{\hat{q}}{J} = \frac{1}{J}[\rho, \rho u_1, \rho u_2, \rho u_3, \rho e]^t \tag{2}$$

$$\bar{E}_m \equiv \text{inviscid flux}$$

$$= (1/J)[\partial_k \xi^m \hat{E}_k]^t$$

$$= (1/J)[\rho U_m, \rho u_1 U_m + \partial_1 \xi^m p, \rho u_2 U_m + \partial_2 \xi^m p, \rho u_3 U_m + \partial_3 \xi^m p, (\rho e + p) U_m]^t, \qquad m = 1,2,3 \tag{3}$$

$$(\bar{E}_v)_2 \equiv \text{viscous and head-conduction flux in } \xi^2 \text{ direction}$$

$$= (1/J)[0, \partial_k \xi^2 \tau_{k1}, \partial_k \xi^2 \tau_{k2}, \partial_k \xi^2 \tau_{k3}, \partial_k \xi^2 (u_n \tau_{kn} - q_k)]^t \tag{4}$$

$$(\bar{E}_v)_3 \equiv \text{viscous and head-conduction flux in } \xi^3 \text{ direction}$$

$$= (1/J)[0, \partial_k \xi^3 \tau_{k1}, \partial_k \xi^3 \tau_{k2}, \partial_k \xi^3 \tau_{k3}, \partial_k \xi^3 (u_n \tau_{kn} - q_k)]^t \tag{5}$$

$$U_m = \partial_k \xi^m u_k \tag{6}$$

The first element of the three momentum elements of Eq. (5) is given by

$$\partial_k \xi^3 \tau_{k1} \equiv \frac{M_\infty \mu}{Re}\left(\psi \partial_1 \xi^3 + \phi \frac{\partial u_1}{\partial \xi^3}\right) \tag{7}$$

where

$$\phi = \partial_k \xi^3 \partial_k \xi^3, \qquad \psi = \tfrac{1}{3} \partial_k \xi^3 \frac{\partial u_k}{\partial \xi^3} \tag{8}$$

The second and third elements of the momentum elements are obtained by replacing the subscript 1, everywhere in Eq. (7), with 2 and 3, respectively. The last element of Eq. (5) is given by

$$\partial_k \xi^3 (u_n \tau_{kn} - q_k) \equiv \frac{M_\infty \mu}{Re}\left\{\psi W + \phi\left[\tfrac{1}{2}\frac{\partial}{\partial \xi^3}(u_1^2 + u_2^2 + u_3^2) + \frac{1}{(\gamma - 1)P_r}\frac{\partial (a^2)}{\partial \xi^3}\right]\right\} \tag{9}$$

where

$$W = \partial_n \xi^3 u_n \tag{10}$$

For Eq. (4), in the case of double thin-layer, Navier-Stokes equations, the elements are given by equations similar to Eqs. (7–10) with the exception of replacing $\xi^3$ by $\xi^2$. The double thin-layer, Navier-Stokes equations are used only for the passive control of flow asymmetry since the existence of the fin creates a second thin layer that is perpendicular to the cone thin layer. The reference parameters for the dimensionless form of the equations are $L$, $a_\infty$, $L/a_\infty$, $\rho_\infty$, and $\mu_\infty$ for the length, velocity, time, density, and molecular viscosity, respectively. The Reynolds number is defined as $Re = \rho_\infty V_\infty L/\mu_\infty$, and the pressure $p$ is related to the total energy per unit mass and density by the gas equation

$$p = (\gamma - 1)\rho\,[e - \tfrac{1}{2}(u_1^2 + u_2^2 + u_3^2)] \tag{11}$$

The viscosity is calculated from the Sutherland law

$$\mu = T^{3/2}\left(\frac{1 + C}{T + c}\right), \quad C = 0.4317 \tag{12}$$

and the Prandtl number $P_r = 0.72$.

In Eqs. (1–10), the indicial notation is used for convenience. Hence, the subscript $k$ and $n$ are summation indices, the superscript or subscript $s$ is a summation index, and the super-

script or subscript $m$ is a free index. The range of $k$, $n$, $s$, and $m$ is 1-3, and $\partial_k \equiv (\partial/\partial_{x_k})$.

Boundary conditions are explicitly implemented. They include inflow-outflow conditions and solid-boundary conditions. At the plane of geometric symmetry, periodic conditions are used for symmetric or asymmetric flow applications on the whole computational domain (right and left domains). At the far-field inflow boundaries, freestream conditions are specified since we are dealing with supersonic flows, whereas at the far-field outflow boundaries, first-order extrapolation from the interior points is used. On the solid boundary, the no-slip and no-penetration conditions are enforced; $u_1 = u_2 = u_3 = 0$, and the normal pressure gradient is set equal to zero. For the temperature, the adiabatic boundary condition is enforced on the solid boundary. The initial conditions correspond to the uniform flow with $u_1 = u_2 = u_3 = 0$ on the solid boundary.

For the passive control applications using a vertical fin in the leeward plane of geometric symmetry, solid-boundary conditions are enforced on both sides of the fin.

## Highlights of Computational Schemes

The first computational scheme used to solve the unsteady compressible, single or double thin-layer, Navier-Stokes equations is based on the Roe inviscid flux-difference splitting scheme. In this scheme, the Jacobian matrices of the inviscid fluxes, $A_s = (\partial \bar{E}_s/\partial q)$, $s = 1$-3, are split into left and right fluxes according to the signs of the eigenvalues of the inviscid Jacobian matrices. Flux limiters are used to dampen the numerical oscillations in regions of large changes of the gradients of the flowfield vector. The viscous and heat transfer terms are centrally differenced. The resulting equation is solved by using approximate factorization in the $\xi^1$, $\xi^2$, and $\xi^3$ directions. The computational scheme is coded in the computer program CFL3D.

The second computational scheme is an implicit, approximately factored, centrally differenced, finite-volume scheme.[22] Added second-order and fourth-order dissipation terms are used in the difference equation on its right-hand side terms, which represent the explicit part of the scheme. The Jacobian matrices of the implicit operator on the left-hand side of the difference equation are centrally differenced in space, and implicit second-order dissipation terms are added for the scheme stability. The left-hand side operator is approximately factored, and the difference equation is solved in three sweeps in the $\xi^1$, $\xi^2$, and $\xi^3$ directions, respectively. The computational scheme is coded in the computer program ICF3D. The ICF3D code is used to verify some of the applications of the

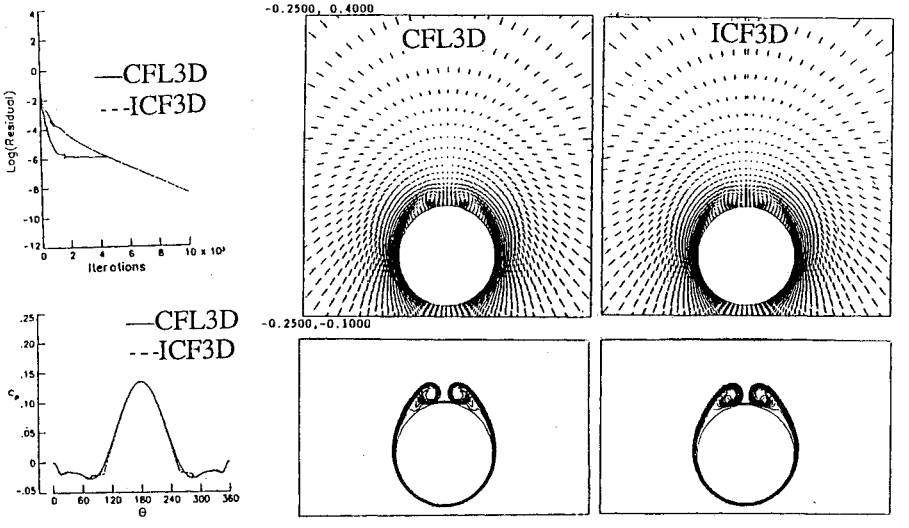


**Fig. 1 Symmetric flow solutions for a circular cone, $\alpha = 10$ deg, $M_\infty = 1.8$, $Re = 10^5$ (validation case).**

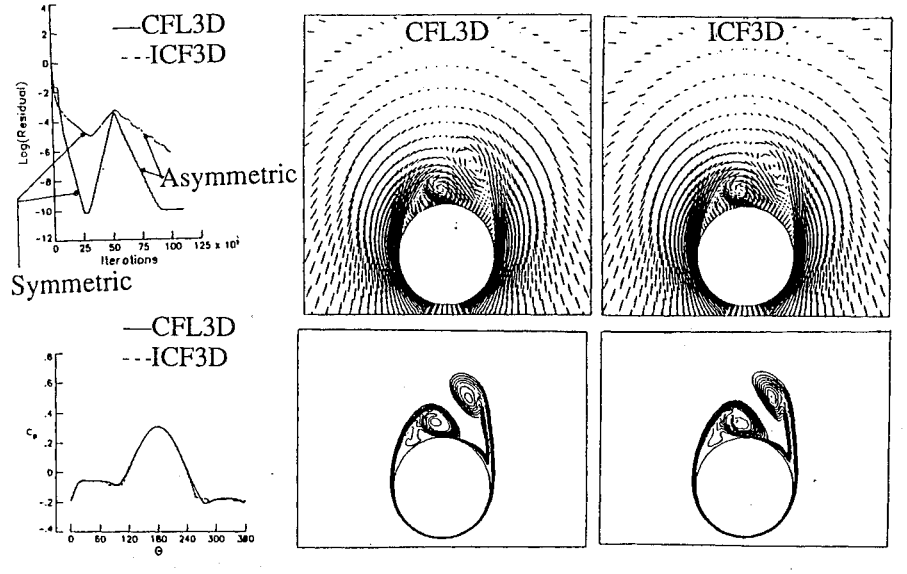


**Fig. 2 Steady asymmetric flow solutions for a circular cone due to random disturbances, $\alpha = 20$ deg, $M_\infty = 1.8$, $R_e = 10^5$ (validation case).**

CFL3D code; namely the cases of Figs. 1 and 2. For the problem of passive control of flow asymmetry, the double thin-layer, Navier-Stokes equations have been solved using the CFL3D code.

Since the applications in this paper cover local-conical flows only, the three-dimensional scheme is used to solve for locally conical flows. This is achieved by forcing the conserved components of the flow vector field to be equal at two planes of $x = 0.95$ and 1.0. The validity of local-conical-flow assumption is discussed in the next section.

## Validity of the Local-Conical-Flow Assumption

The solutions presented in this paper are called local-conical solutions, which are obtained by equating the conserved components of the flowfield vector, in the three-dimensional scheme, on two crossflow planes that are in close proximity to each other at a selected location. Once this location is specified ($x = 1.0$ in the present applications), the flow Reynolds number is determined and the time scale, for time-accurate solutions, is also determined. The resulting solution is a local-conical solution at the specified location. It is not a global-conical solution. The locally conical equations can be shown by considering the conservative form of the Navier-Stokes equations in the Cartesian system

$$\frac{\partial q}{\partial t} + \frac{\partial (E - E_v)_i}{\partial x_i} = 0, \qquad i = 1 - 3 \tag{13}$$

By introducing the conical coordinates

$$\eta_1 = \frac{x_1}{x_3}, \qquad \eta_2 = \frac{x_2}{x_3}, \qquad \eta_3^2 = x_i x_i \tag{14}$$

and using the chain rule to express Eq. (13) in terms of the conical coordinates, we get

$$\frac{\eta_3}{\theta}\frac{\partial q}{\partial t} + \frac{\partial}{\partial \eta_1}(\bar{E} - \bar{E}_v)_1 + \frac{\partial}{\partial \eta_2}(\bar{E} - \bar{E}_v)_2 + \frac{\eta_3}{\theta^2}\frac{\partial}{\partial \eta_3}(\bar{E} - \bar{E}_v)_3 + 2(\bar{I} - I_v) = 0 \tag{15}$$

where

$$\theta = \sqrt{1 + \eta_1^2 + \eta_2^2}$$

$$\bar{E}_1 = E_1 - \eta_1 E_3, \quad \bar{E}_2 = E_2 - \eta_2 E_3$$

$$\bar{E}_3 = E_3 + \eta_1 E_1 + \eta_2 E_2$$

$$\bar{I} = \bar{E}_3 \tag{16}$$

$$\bar{E}_{v1} = E_{v1} - \eta_1 E_{v3}$$

$$\bar{E}_{v2} = E_{v2} - \eta_2 E_{v3}$$

$$\bar{E}_{v3} = E_{v3} + \eta_1 E_{v1} + \eta_2 E_{v2}$$

$$I_v = \bar{E}_{v3} \tag{17}$$

The conical flow condition requires that the flow variables be independent of the coordinate $\eta_3$. If this condition is imposed in Eq. (15), by dropping the derivatives with respect to $\eta_3$, the equation reduces to

$$\frac{\eta_3}{\theta}\frac{\partial q}{\partial t} + \frac{\partial}{\partial \eta_1}(\bar{E} - \bar{E}_v)_1 + \frac{\partial}{\partial \eta_2}(\bar{E} - \bar{E}_v)_2 + 2(\bar{I} - I_v) = 0 \tag{18}$$

It is clearly seen that Eq. (18) still has $\eta_3$ dependence in the unsteady term and the viscous and heat-flux terms (one can see the explicit dependence of the viscous and heat-flux terms on $\eta_3$ by transforming the elements of these vectors to the conical coordinates). Hence, Eq. (18) is not self-similar, and therefore it does not represent a global-conical flow. However, if $\eta_3$ is set equal to a constant $c$, then one can consider Eq. (18) to represent a local-conical flow around $\eta_3 = c$. The resulting solution using Eq. (18) with $\eta_3 = c$ represents a local-conical solution with a Reynolds number and a time that are scaled by the constant $c$. It should be noted that if the flow is steady and inviscid, then Eq. (18) becomes self-similar, and hence it represents a global-conical flow. In the present paper, we indirectly solve Eq. (18) at a fixed location of unity. This is achieved in the three-dimensional flow equation, Eq. (1), by equating the elements of the flowfield vector at two planes in close proximity to each other. In this paper, we selected these planes to be located at $x = 0.95$ and 1.0. In other numerical experiments, we use the plane locations at $x = 0.995$ and 1.0. The results of these experiments were in excellent agreement with those of the present paper.

## Computational Studies

Supersonic flows about a 5 deg semiapex angle circular cone at a Reynolds number of $10^5$ have been considered. A grid of $161 \times 81$ points in the circumferential and normal directions is used throughout the present applications. The grid is generated by using a modified Joukowski transformation with a geometric series for the grid clustering near the solid boundary. The minimum grid length is $10^{-4}$ at the solid boundary, and the maximum radius of the computational domain is $21r$, where $r$ is the radius of the circular cone at the axial station of unity.

### Steady Symmetric Flows

Figure 1 shows steady symmetric vortical-flow solutions for the circular cone at 10 deg angle of attack and 1.8 freestream Mach number. In the figure, we show comparisons of the results of the CFL3D and ICF3D codes. The results include the residual error versus the number of iterations, the crossflow velocity, the total-pressure-loss contours, and the surface-pressure coefficients. It should be noted here that the angle $\theta$ in the $C_p$ figure is measured from the leeward plane of geometric symmetry in the clockwise direction. The agreement of the results of the two code is excellent, and the results are in full agreement with those of Siclari and Marconi.[20]

### Steady Asymmetric Flow

*Round-Off and Truncation Error Disturbances*

The cone angle of attack is increased to 20 deg while all the other flow conditions are kept fixed. Figure 2 shows the results of the CFL3D and ICF3D codes. In the residual error figure, the CFL3D code shows that the residual error drops 10 orders of magnitude within 2500 iteration steps. Thereafter, the error increases by six orders of magnitude. The flow is symmetric during this 5000 iteration steps. Next, the error drops down by another six orders of magnitude and stays constant for 2500 iteration steps. The flow becomes asymmetric and stable. The ICF3D code shows that the residual error drops five orders of magnitude in the first 3000 iteration steps, increases two orders of magnitude in the next 2000 iteration steps, and then drops down by three orders of magnitude within the next 5000 iterations. The flow solution goes through a symmetric unstable solution and then to an asymmetric stable solution. The pressure-coefficient figure for the two codes is the same over the full range of the circumferential angle $\theta$. The suction pressure in the range of $\theta = 0$-90 deg is lower than that of the range of $\theta = 270$-360 deg. The crossflow velocity and total-pressure-loss contours for the two codes are also in excellent agreement. They show the nature of the flow asymmetry and its details. The results are in complete agreement with those of Ref. 20.

Since the residual error of the CFL3D code is much smaller than that of the ICF3D code after the first 2500 iterations, the disturbance that triggered the asymmetry in the first code is attributed to the machine round-off error, while the distur-

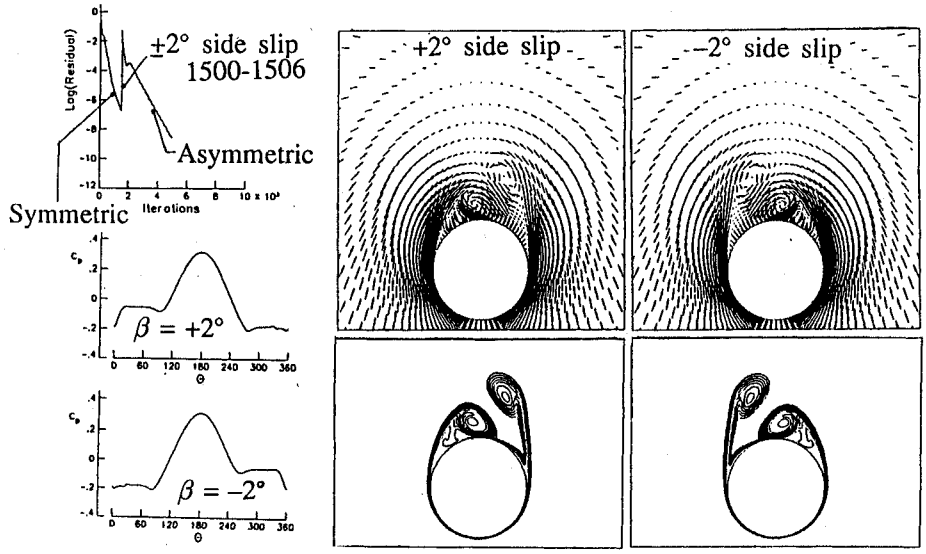


Fig. 3 Steady asymmetric flow solutions for a circular cone due to ±2 deg transient side slip, $\alpha = 20$ deg, $M_\infty = 1.8$, $R_e = 10^5$.

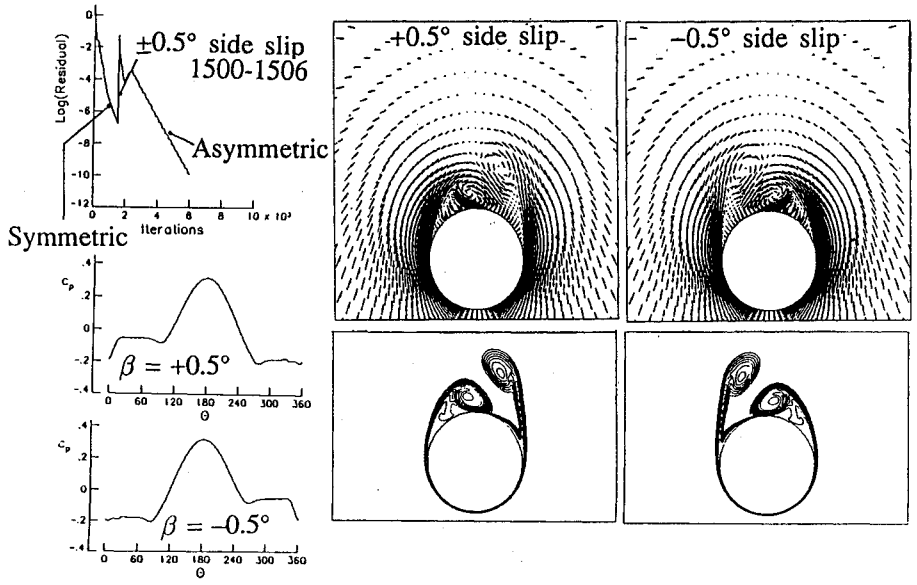


Fig. 4 Steady asymmetric flow solutions for a circular cone due to ±5 deg transient side slip, $\alpha = 20$ deg, $M_\infty = 1.8$, $R_e = 10^5$.

bance that triggered the asymmetry in the second code is attributed to the truncation error of the scheme (since there is a bias due to the spatial marching direction). Both disturbances are random in nature. However, irrespective of the source of disturbance, the final asymmetric stable solution is the same.

*Controlled Transient Side-Slip Disturbances*

In Figs. 3 and 4, we show steady asymmetric flow solutions due to transient side-slip disturbances of ± 2 and ± 0.5 deg. The residual-error figures show a drop of seven orders of magnitude in the first 2000 iterations. At this step, a side-slip disturbance is imposed for six iteration steps, then it is removed. Irrespective of the magnitude or the sign of the side-slip disturbance, the residual error increases by six orders of magnitude, then it drops down very rapidly. A stable asymmetric flow solution is obtained. The asymmetric solutions corresponding to the ± 2 deg side-slip disturbances are mirror images of each other, as can be seen from the figures of the surface-pressure coefficient, crossflow velocity, and total-pressure-loss contours. The corresponding asymmetric solutions with the ± 0.5 deg side-slip disturbances are exactly the same as those of the ± 2 deg side-slip disturbances. Moreover, the final asymmetric solutions of the ± 2 deg and ± 0.5 deg side-slip disturbances are the same as those of Fig. 2.

Again, this numerical experiment shows that the same physical flow asymmetry is obtained.

**Unsteady Asymmetric Vortex Shedding**

In the present case, the angle of attack is increased to 30 deg and all the other flow conditions are kept the same as those of the cases above. Figure 5 shows the results of this case.

Here, we show the history of the residual error and the lift coefficient up to the 15,700 time step. First, pseudo-time stepping was used up to 10,000 iterations, and the solution was monitored every 500 iterations. The solution showed that the asymmetry was changing from the left side to the right side, which indicated a possibility of unsteady asymmetric vortex shedding. The residual error was also oscillating. The computations were repeated starting from the 3,500 iteration step using time-accurate calculations with $\Delta t = 10^{-3}$. The residual-error and lift-coefficient figures show the time history of the solution. It is seen that the residual error and the lift coefficient show a transient response that is followed by a periodic response. Figure 5 shows also snapshots of the time history of the solution for the total-pressure-loss contours and surface-

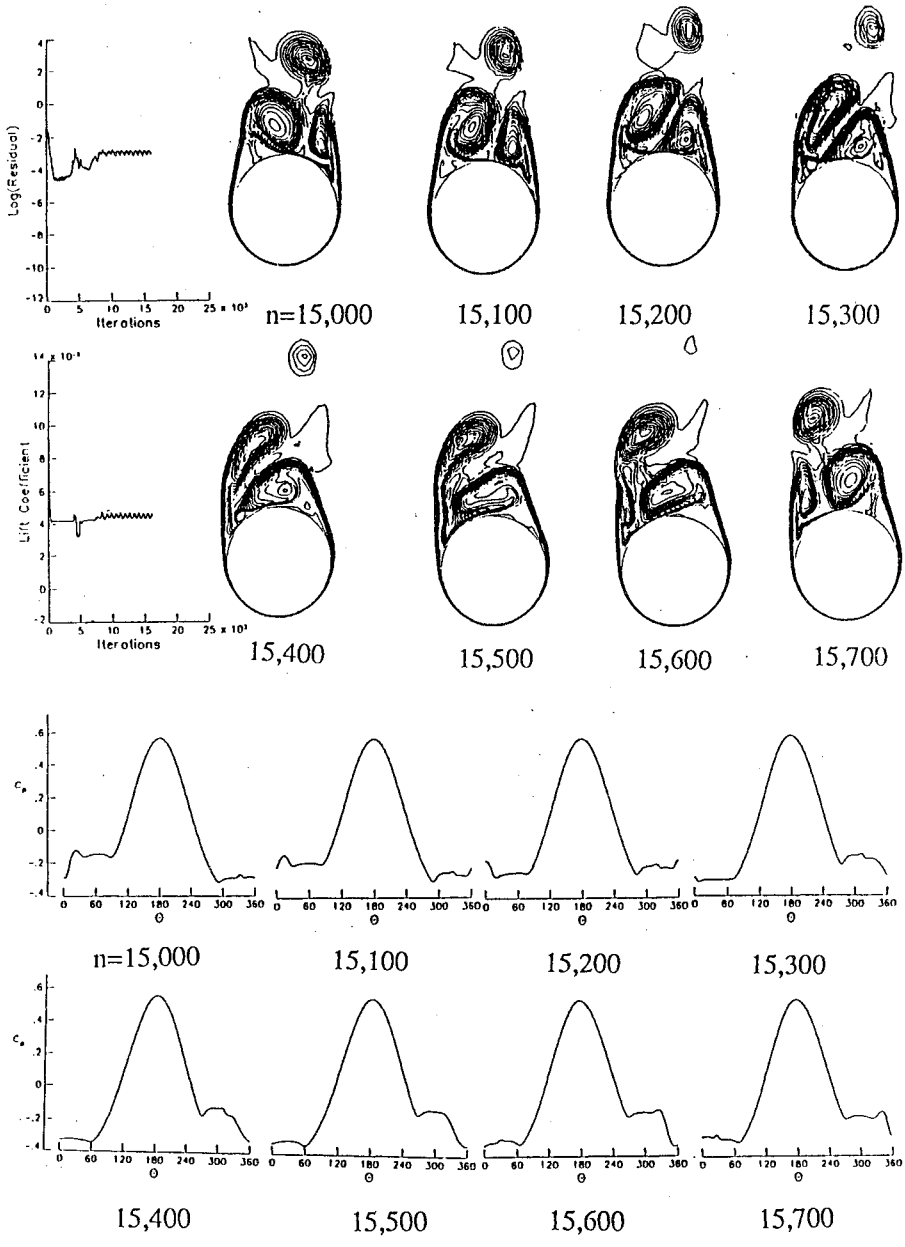


**Fig. 5 Unsteady asymmetric flow solution (using flux-difference splitting) with vortex shedding for a circular cone during periodic flow responses; $\alpha = 30$ deg, $M_\infty = 1.8$, $R_e = 10^5$, $\Delta t = 10^{-3}$.**

pressure coefficient. The solutions are shown every 100 time steps starting from the time step of 15,000. At $n$ = 15,000, the asymmetric flow is seen with an already shed vortex from the right side. As time passes, the shed vortex is convected in the flow and the primary vortex on the left side stretches upwards while the primary vortex on the right gets stronger, as it is seen from the surface pressure figures. At $n$ = 15,600, the primary vortex on the left side is about to be shed. At $n$ = 15,700, the primary vortex on the left side is shed in the flowfield. It should be noticed that the solution at $n$ = 15,700 is exactly a mirror image to that at $n$ = 15,000. The solution from 15,000-15,700 represents the first one-half the cycle of shedding. The solution from 15,700–16,400 (not shown) represents the second one-half the cycle. The periodicity of the shedding motion is conclusively captured. The period of oscillations is $10^{-3} \times$ 1,400 steps = 1.4 that produces a shedding frequency of 4.400 (Strouhal number). This solution is obtained by using the flux-difference splitting (FDS) scheme.

Very recently, a researcher in the computational simulation area of asymmetric flows claimed that he had applied the flux-vector splitting (FVS) scheme of the CFL3D code to the present flow case. His solution showed that the flow was steady and symmetric. A statement of his results was communicated to us and we were asked to respond. Therefore, we recomputed the present flow case using the FVS scheme of the same CFL3D code. In Fig. 6, we show the results of the time-accurate solutions using the FVS scheme using the same grid. Using the FVS scheme, the flux limiters were turned on, and as can be seen from the logarithmic-residual curve, the solution becomes symmetric and steady after 5000 time steps. Next, the flux limiters are turned off, and the solution shows a transient response up to 12,000 time steps. Thereafter, the solution becomes periodic with periodic asymmetric vortex shedding. The solution was monitored every 100 time steps, and the results from $n$ = 13,900–14,600 are shown. Although the process of adjusting the time instants is difficult to match those of the FDS solution, it is seen that the captured snapshots of the FVS solution almost match those of the FDS solution. Comparing the FVS solutions at $n$ = 13,900 and 14,600, it is seen that they are mirror images of each other. Hence, periodic flow response has been achieved with a period of $1400 \times 10^{-3} = 1.4$, which is exactly the same period of shedding as that of the FDS solution. This pinpoints the high numerical dissipation effect of the FVS scheme when the flux

limiters are turned on. The resulting numerical dissipation in the FVS is large enough to dampen the random disturbances of the flow solution. By turning off the flux limiters in the FVS scheme, the random disturbances can grow, producing the asymmetric unsteady vortex shedding. This also shows that the FDS scheme, even with the flux limiters turned on, is less dissipative than the FVS scheme. These results conclusively explain the erroneous claim of steady flow made by the previously mentioned researcher.

**Steady Asymmetric Flow at Different Mach Numbers (Effect of $M_\infty$)**

Figure 7 shows the effect of the freestream Mach number ($M_\infty = 2.2$, 2.6, and 3.0) on the convergence history, surface pressure, crossflow velocity, and total-pressure-loss contours for the circular cone at 20 deg angle of attack. At $M_\infty = 2.2$, the residual error shows that the stable asymmetric flow is obtained within the same number of iterations as that of the $M_\infty = 1.8$ case. At $M_\infty = 2.6$, the residual error shows that the stable asymmetric flow is obtained after a large number of iterations. And at $M_\infty = 3.0$, no asymmetric flow was captured, the flow stayed symmetrically stable. The surface pressure figures show that the asymmetry gets weaker as the Mach number is increased. This conclusion is clearly seen from the crossflow velocity and the total-pressure-loss figures. It should be noted that since the nature of disturbance is random, flow asymmetry changes sides as the Mach number increases until it disappears.

**Passive Control of Flow Asymmetry**

Figure 8 shows the passive control of flow asymmetry by inserting a vertical fin in the leeward plane of geometric symmetry. The fin height is equal to the cone local radius $r$. Here, the double thin-layer, Navier-Stokes equations are used to obtain these results. The flow Mach number is kept at 1.8 and the angle of attack is 20 deg. The flow is completely symmetric as can be seen from the figures of the surface-pressure coefficient, total-pressure-loss contours, and crossflow velocity. A blow-up of the cross-flow velocity at the fin-cone juncture shows two corner recirculating bubbles of exactly the same size. This case has been obtained after 24,000 iteration steps. Again, this is the first time such a computational simulation of

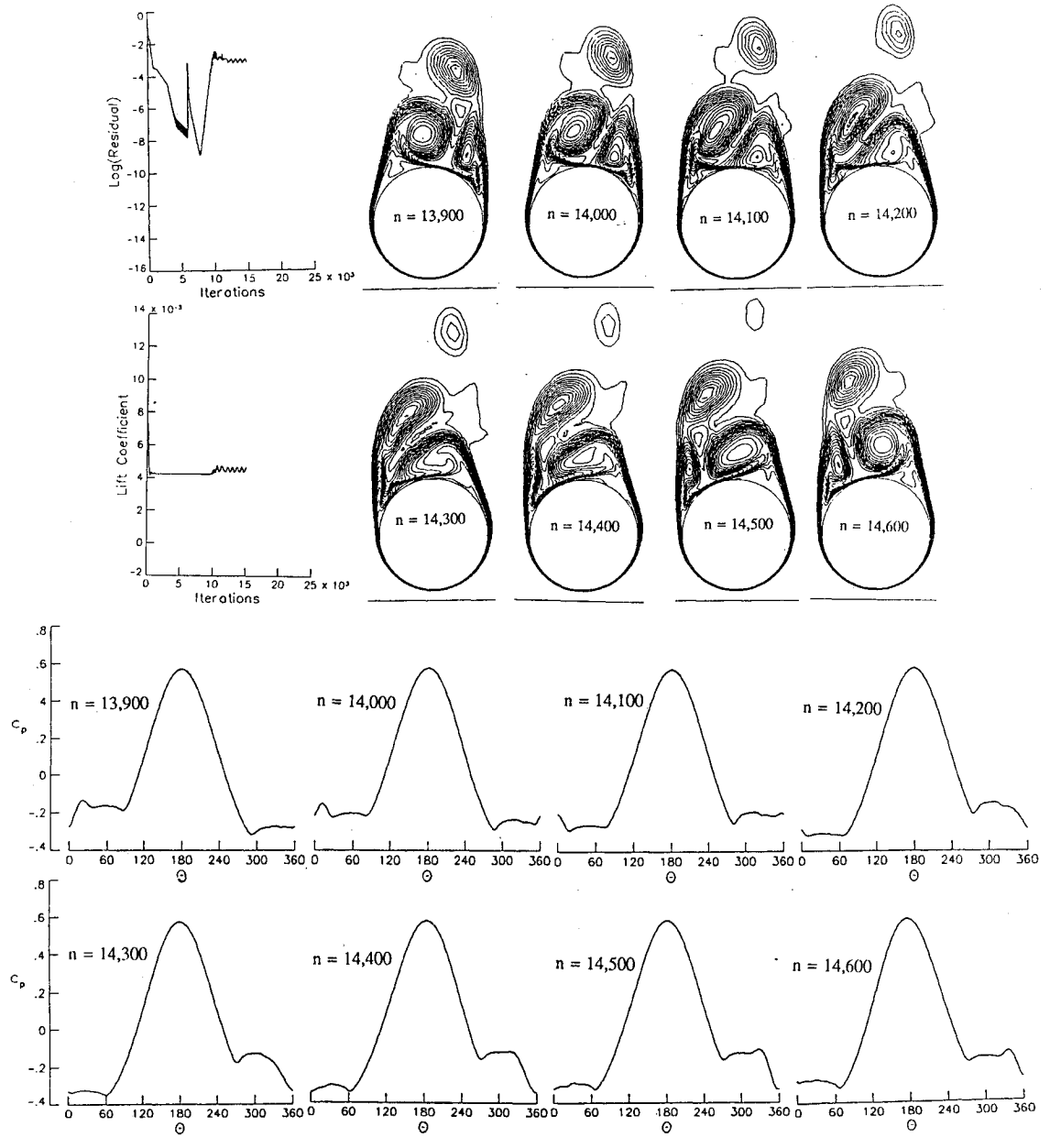


**Fig. 6 Unsteady asymmetric flow solution (using flux-vector splitting) with vortex shedding for a circular cone during periodic flow response; $\alpha = 30$ deg, $M_\infty = 1.8$, $R_e = 10^5$, $\Delta t = 10^{-3}$.**

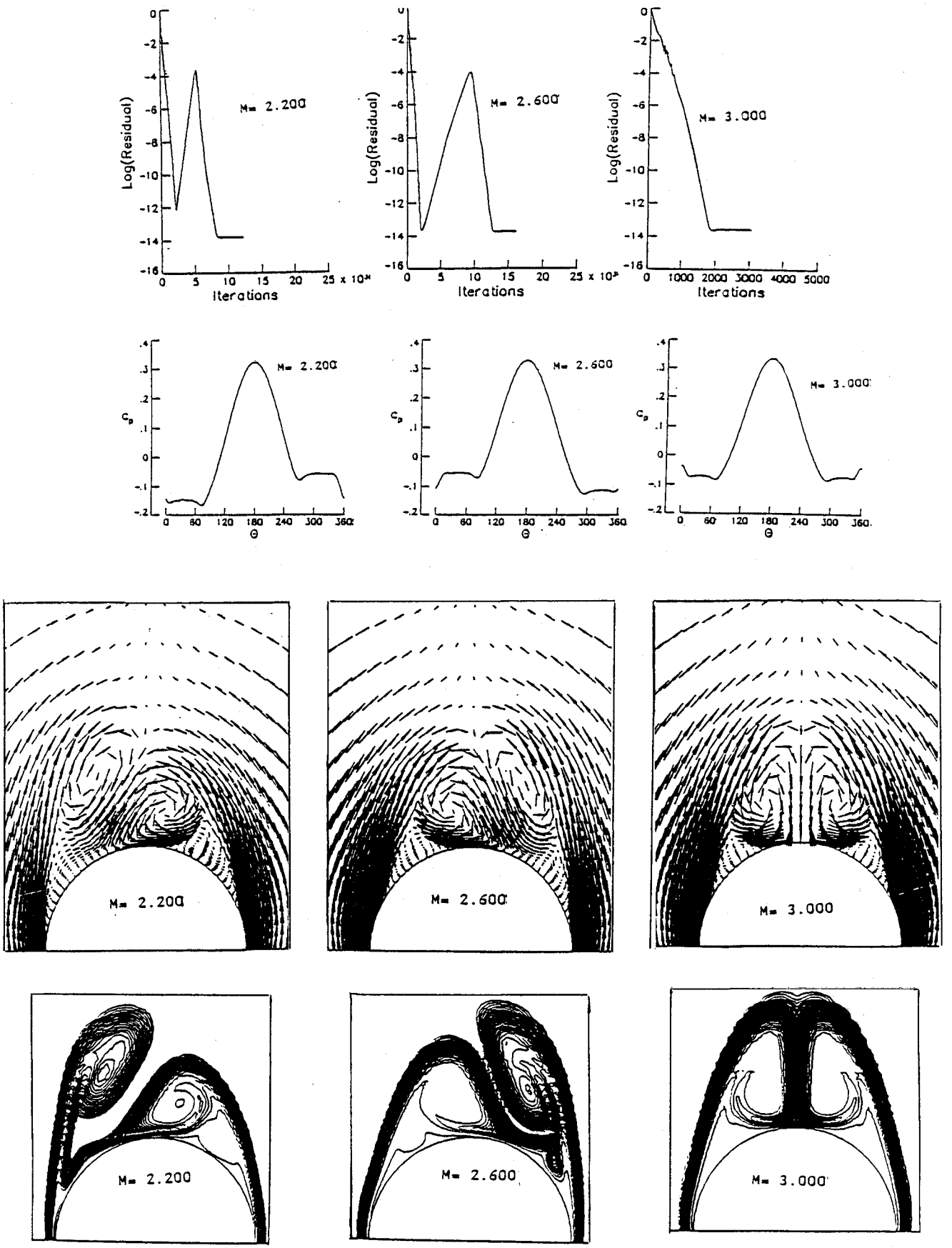


Fig. 7 Effect of the freestream Mach number on the flow asymmetry for a circular cone, $\alpha = 20$ deg; $M_\infty = 2.2, 2.6, 3.0$; $R_e = 10^5$.

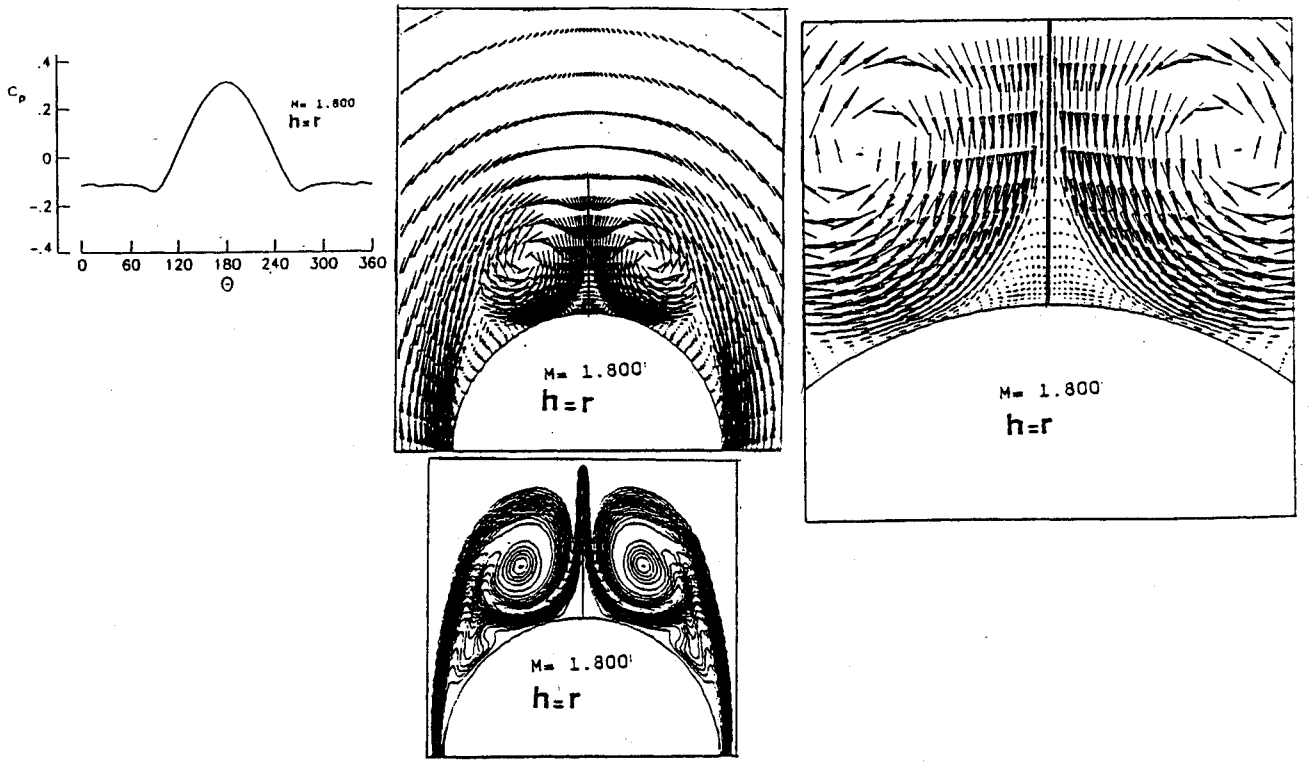


**Fig. 8 Control of asymmetric flow of a circular cone using a vertical fin in the leeward geometric plane of symmetry, $\alpha = 20$ deg, $M_\infty = 1.8$, $R_e = 10^5$, h = r ($r \equiv$ radius of circular section).**

the passive control of the flow asymmetry has been presented. The results are in full agreement with Stahl's experimental study.[21]

## Concluding Remarks

This paper presents extensive computational study and simulation of steady and unsteady asymmetric vortex flow around circular cones. A systematic study has been carried out to show the effects of angle of attack and Mach number. The study shows that the flow asymmetry is independent of the type or level of the disturbance. For the controlled transient side-slip disturbance, the solution is unique. For the uncontrolled random disturbance, the solution is also unique with the exception of having the same asymmetry changing sides on the cone. It conclusively shows that periodic vortex shedding has been captured at larger angles of attack. The unsteady asymmetric vortex-shedding solution has been substantiated by using two different computational schemes. It also shows that as the Mach number increases, the vortex flow asymmetry gets weaker until it disappears. The possibility of passive control of flow asymmetry has also been demonstrated. Many of the cases presented here are obtained for the first time, in particular, the asymmetric vortex shedding cases and the cases of passive control of flow asymmetry.

## Acknowledgment

This research is supported by the NASA Langley Research Center under Grant NAS1-18584-08 for the first two authors.

## References

[1]Thomas, K. D., and Morrison, D. F., "The Spacing, Position and Strength of Vortices in the Wake of Slender Cylindrical Bodies at Large Incidence," *Journal of Fluid Mechanics*, Vol. 50, No. 4, 1971, pp. 751-783.

[2]Keener, E. R., and Chapman, G. R., "Similarity in Vortex Asymmetrics Over Slender Bodies and Wings," *AIAA Journal*, Vol. 15, No. 9, 1988, pp. 1370-1372.

[3]Peake, D. J., Owen, F. K., and Higuchi, H., "Symmetrical and Asymmetrical Separations About a Yawed Cone," AGARD-CP-247, Jan. 1979, pp. 16.1-16.27.

[4]Peak, D. J., Fisher, D. F., and McRae, D. S., "Flight, Wind Tunnel and Numerical Experiments with a Slender Cone at Incidence," *AIAA Journal*, Vol. 20, No. 10, 1979, pp. 1338-1345.

[5]Peake, D. J., and Tobak, M., "Three-Dimensional Flows About Simple Components at Angle of Attack," *High Angle-of-Attack Aerodynamics*, AGARD LS-121, Aug. 1982, pp. 2.1-2.56.

[6]Skow, A. M., and Peake, D. J., "Control of the Forebody Vortex Orientation by Asymmetric Air Injection, (Part B)—Details of the Flow Structure," *High Angle-of-Attack Aerodynamics*, AGARD-LS-121, Aug. 1982, pp. 10.1-10.22.

[7]Nishioka, M., and Sato, H., "Mechanism of Determination of the Shedding Frequency of Vortices Behind a Cylinder at Low Reynolds Numbers" *Journal of Fluid Mechanics*, Vol. 89, Part 1, 1978, pp. 49-60.

[8]Lamont, P. J., "Pressures Around an Inclined Ogive Cylinder with Laminar, Transitional, or Turbulent Separation," *AIAA Journal*, Vol. 20, No. 11, November 1980, pp. 1492-1499.

[9]Lamont, P. J., "The Complex Asymmetric Flow Over a 3.5D Ogive Nose Cylindrical Afterbody at High Angles of Attack," AIAA Paper 82-0053, Jan. 1982.

[10]Yanta, W. J., and Wardlaw, A. B., Jr., "The Secondary Separated Region on a Body at High Angles-of-Attack," AIAA Paper 82-0343, January 1982.

[11]Ericsson, L. E., and Reding, J. P., "Vortex-Induced Asymmetric Loads, in 2-D and 3-D Flows," AIAA Paper 80-0181, Jan. 1980.

[12]Shanks, R. E., "Low Subsonic Measurements of Static and Dynamic Stability Derivatives of Six Flat Plate Wings Having Leading-Edge Sweep Angles of 70°-84°," NASA TN D- 1822, July 1963.

[13]Rediniotis, O., Stapountzis, H. and Telionis, D. P., "Vortex Shedding Over Nonparallel Edges," Virginia Polytechnic Institute and State University, Blacksburg, VA, Engineering Rept. VPI-88-39, Dec. 1988.

[14]McRae, D., "Numerical Study of Supersonic Viscous Cone Flow at High Angle of Attack," AIAA Paper 76-0097, Jan. 1976.

[15]Bluford, G., and Hankey, W., "Numerical Solutions of Supersonic and Hypersonic Viscous Flow Around Thin Delta Wings," *Proceedings of the AIAA 22nd Structural Dynamics Conference*, AIAA, New York, 1979, pp. 793-810.

[16]Graham, J. E., and Hankey, W. L., "Computation of the Asymmetric Vortex Pattern for Bodies of Revolution," *AIAA Journal*,

Vol. 23, No. 11, 1983, pp. 1500–1504.
[17]Degani, D., and Schiff, L. B., "Numerical Simulation of the Effect of Spatial Disturbances on Vortex Asymmetry," AIAA Paper 89-0340, Jan. 1989.
[18]Marconi, F., "Asymmetric Flows About Sharp Cones in a Supersonic Stream," *Proceeedings of the 11th International Conference on Numerical Methods in Fluid Dynamics,* Williamsburg, VA, June 1988.
[19]Dyer, D., Fiddes, S. P., and Smith, J. H. B., "Asymmetric Vortex Formation from Cones at Incidence—A Simple Inviscid Model," *Aeronautical Quarterly*, Vol. 33, June 1982, pp. 293–312.
[20]Siclari, M. J., and Marconi, F., "The Computation of Navier-Stokes Solutions Exhibiting Asymmetric Vortices," AIAA Paper 89-1817, June 1989.
[21]Stahl, W., "Suppression of Asymmetry of Vortex Flow Behind a Circular Cone at High Incidence," AIAA Paper 89-3372-CP, Aug. 1989.
[22]Kandil, O. A., and Chuang, H. A, "Unsteady Navier-Stokes Computations Past Oscillating Rolling Delta Wings at High Incidences," AIAA Paper 89-081, Jan. 1989.